Supporting Information

Enhancing Specificity in the Janus Kinases: A Study on the Thienopyridine JAK2 Selective Mechanism Combined Molecular Dynamics Simulation

Jiao Jiao Li, Peng Cheng, Jing Tu, Hong Lin Zhai*, Xiao Yun Zhang

College of Chemistry & Chemical Engineering, Lanzhou University, Lanzhou, 730000, PR China

1. Supplementary material for four complexes 19-JAK.

Four hydrogen bonds for the complex **19**-JAK2 was superior to others (for **19**-JAK1 with three hydrogen bonds, for **19**-JAK3 with two hydrogen bonds and for **19**-TYK2 one hydrogen bond). The differences in the number of hydrogen bonds was one of the JAK2 selectivity factors.

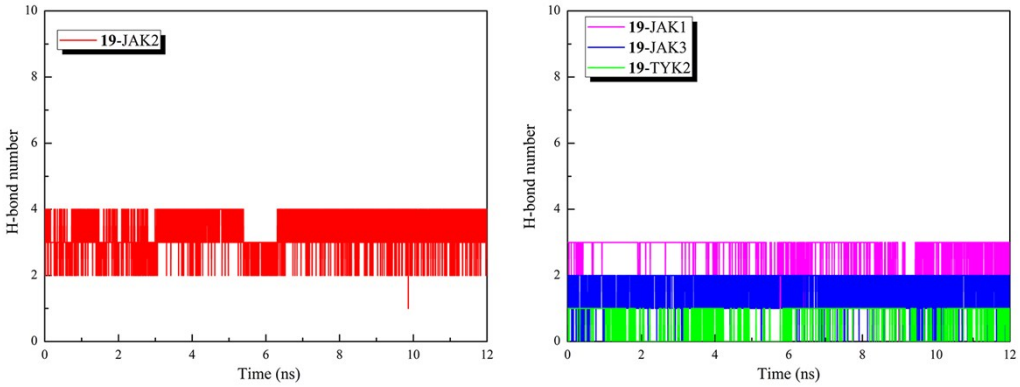

Fig. S1 Numbers of hydrogen bonds *vs.* simulation time for (a) **19**-JAK2 (b) **19**-JAK1, **19**-JAK3 and **19**-TYK2.

2. Results and discussion for four 22-JAK members

2.1. Molecular docking

As shown in the molecular docking results, the performance of molecular docking was well validated and the initial structures with the best recognition poses were obtained to further execute

* Correspondence to: Tel.: +86 931 8912596; fax: +86 931 8912582; E-mail address: zhaihl@163.com (H.L. Zhai).

MD simulations. From the satisfying superimposition between the crystal structure of 3TJD and the re-docking conformation of JAK2 with inhibitor **22** by the RRD protocol (Fig.1), the root mean square deviation (RMSD) value between them was 0.580Å. In addition, the docking scores of four **19**-JAK members were highly consistent with each of them experimental activity (Table S1), which also justified that the JAK2 inhibitor **22** demonstrated the high JAK family selectivity. It fully turned out that the molecular docking method was feasible.

2.2. MD simulations

2.2.1. Stability of the system simulations

After docking process, the MD simulations of eight systems during 12 ns were run to monitor the dynamic, structural and energetic properties. The temporal root mean square deviation (RMSD) values of the C_α atoms of residues within 5 Å around the ligand in the binding pocket relative to the respective initial structures were shown in the Fig. S2. It was shown that the RMSD fluctuation of each system was always very small during the MD simulations. Furthermore, the time evolution of the RMSD values for all protein backbone atoms for each system relative to their initial structures also tended to converge specially during the last 6 ns (Fig. S2). The convergent results suggested that all system simulations reached equilibrium and stabilization during the last 6 ns, which confirmed that the selection of the initial conformations was reasonable. Therefore, we could employ the last stable 3 ns trajectories for the following energy calculations.

2.2.2. Selectivity analysis for four **22**-JAK members

To validate and convince the findings further, the inhibitor **22** that had the same thienopyridine scaffold and the similar JAK2 inhibition selectivity was bound dynamically into four JAK kinases to analyze the JAK2 selectivity over JAK1, JAK3 and TYK2. Judging from the

energy calculation results by the MM/GBSA approach (Table S2), the predicted energies gone along with their experimental activities and varied from -56.92 to -39.23 kcal/mol, and the binding energy differences (ΔΔG) of **22**-JAK2 over **22**-JAK1, **22**-JAK3 and **22**-TKK2 were 13.29 kcal/mol, 17.69 kcal/mol and 16.12 kcal/mol, respectively. From four energy items (ΔE_{vdw}, ΔE_{ele}, ΔG_{GB} and ΔG_{SA}), the main reason why the thienopyridine compound **22** demonstrated high JAK2 selectivity in binding affinities should be the van der Waals interaction term (-57.85 kcal/mol for **22**-JAK2, -48.39 kcal/mol for **22**-JAK1, -49.32 kcal/mol for **22**-JAK3, -48.29 kcal/mol for **22**-TYK2). In all systems, the remarkable nonpolar contributions as the major driving force suggested that the hydrophobic amino acid residues in the active pocket played a crucial role in the ligand binding process, and the polar interactions of positive value were adverse to the integration between JAK family kinases and inhibitors. Interestingly, the electrostatic (ΔE_{ele}) between JAK1 and **22** was counteracted by the unfavorable polar part of desolvation although ΔE_{ele} for **22**-JAK1 was the greater superiority than **22**-JAK2. The nonpolar forces ultimately may be the positive factors of the potent and highly selective thienopyridine JAK2 inhibitors with the long and conjugate scaffold. The modes of **22**-JAK family members were consistent with the corresponding **19**-JAK family members, which further proved that the computational method was reliable to analyze the JAK2 selectivity.

Due to the different size of the ligand-binding cavity for four JAK family members, the selective difference mainly reflected that the long plane scaffold of the inhibitor **22** with the big hydrophobic *t*-butyl group in JAK1, JAK3 and TYK2 site cavities had the different degree of torsion relative to in JAK2 site cavity. Allowing for the degree of JAK2 selectivity over the other JAK family kinases, the comparison of the structural features between **22**-JAK2 and the other

three **22**-JAK members fell into two cases to elaborate the binding differences methodically as follows.

2.2.2.1. The comparison of the structural features between **22**-JAK2 and **22**-JAK1

To deeply dissect the impact of binding mode on JAK2 selectivity, the structural and energetic basis of **22**-JAK interaction was provided to make a comparative analysis in the JAK active site. For the important comparative study between **22**-JAK2 and **22**-JAK1, the structural framework of **22** can be well embedded in the ATP-binding cleft of JAK2 PTK and oriented so that the thienopyridine ring pointed towards the hinge region, the amide group was exposed to the bulk solvent and the *t*-butyl group was located in the glycine loop (Fig. S3a and Fig. S4b). For the complex **22**-JAK1, because of the non-conservative residue His885 at the tip of the glycine loop of JAK1 (Fig. S4a), the cleft of the glycine loop in the collapsed position was narrow so that the *t*-butyl group with a large steric effect deviated from the tip of the glycine loop and was exposed to the bulk solvent (Fig. S3b and Fig. S4c), which leaded to the differences in the individual residue free energy contribution and hydrogen bonding network.

The per-residue energy contributions of four key domains (Fig. S5) suggested that the hinge region served as the important player to JAK2 inhibitory selectivity. Owing to the stronger H-bond network in JAK2 hinge region, the energy difference ($\Delta\Delta G$) of each residue (Fig. S6) shown that their hinge regions were more discrepant than other domains, and that the significantly different equivalence residues were Glu930/Glu957, Tyr931/Phe958, Leu932/Leu959, Gly935/Gly962 and Asn981/Asn1008 for **22**-JAK2/**22**-JAK1. As can be seen from Fig. S3e, the residues Leu855, Val863 from the glycine-rich loop, Met929, Glu930, Tyr931, Leu932, Gly935 from the hinge region and Asn981, Leu983 from the catalytic loop with the major favorable

energy contributions to the complex **22**-JAK2 indicated that they served as major residues for ligand binding. It was interesting that the important residues of the complex **22**-JAK2 and the homologous residues of three other complex members were almost hydrophobic, which can form similarly strong nonpolar interactions with compound **22** (Fig. S7c). Noticeably, the distinct differences of the key residue contributions on 4, 6 and 8 positions (equivalence residues) can be mainly attributed to the variant contributions of the polar interactions (Fig. S7a and S7b), which may be in keeping with hydrogen bonding interactions. A strong hydrogen bonds network for the complex **22**-JAK2 was created that involved residues Glu930 (one H-bond, **22**(N16-H38)···Glu930(O), with 76.80% occupancy), Leu932 (two H-bonds, Leu932(N-H)···**22**(N1) and **22**(N18-H40)···Leu932(O), with 54.93% and 27.80% occupancy, respectively) and Asp994 (one H-bond, **22**(N24-H43)···Asp994(OD1), with 24.07% occupancy). However, it was unsatisfactory that three H-bonds with high occupancies for the complex **22**-JAK1 (**22**(N24-H43)···Glu883(O), Leu959(N-H)···**22**(O30), **22**(N16-H39)···Gly1020(O) and **22**(N16-H38)···Asp1021(OD1), with 84.33%, 18.93%, 57.13% and 77.07% occupancy, respectively) leaded to the relatively strong electrostatic contribution as a result of the relatively poor selectivity (*VS.* JAK2, 43-fold) (Table S3 and Fig. S9).

2.2.2.2. The structural comparison between **22**-JAK2 and two complexes **22**-JAK3 and **22**-TYK2

However, the contrast of JAK2 and the other two kinases JAK3 and TYK2 indicated that the binding orientations of complexes **22**-JAK3 and **22**-TYK2 were all different from that of the complex **22**-JAK2. In the ATP-binding cleft of JAK3 and TYK2 PTKs, one end of the amide group for molecule **22** was buried in the interior of the active cavity adjacent to the hinge region, and the other end of the *t*-butyl group pointed towards the bulk solvent (Fig. S3c and S3d). As

shown in Figure S8, the glycine-rich loop approached the catalytic loop so that the width and height of the active pocket may not be enough to place in the compound **22** with the long scaffold and the hydrophobic *t*-butyl group. The visible discrepancy with the large steric effect won the high levels of JAK2 electivity for **22**-JAK3 (427-fold) and **22**-TYK2 (493-fold). The H-bond information listed in Table 3S suggested that the complex **22**-JAK2 gone with the high H-bond number and occupancy. The results leaded to the weak energy contributions (Fig. S3g and S3h) and hydrogen bonding interactions (Fig. S3c and S3d) (for **22**-JAK3, two H-bonds, **22**(N16-H39)⋯Glu903(O) and Leu905(N-H)⋯**22**(N16) with 50.67% and 17.33% occupancy, for **22**-TYK2, two H-bonds with 16.07% and 42.07% occupancy, 22(N24-H43)⋯Leu983(O) **22**(N16-H38)⋯Glu979(O)). Moreover, their differences in the hinge regions and key residues were almost in line with that of complexes **22**-JAK2 and **22**-JAK1 (Fig. S6 and S7).The results suggest that the compound **22** with the long plane scaffold and the big hydrophobic *t*-butyl group was unable to fit perfectly into the narrow active pocket of JAK3 and TYK2, which may be the critical element in the high-fold JAK2 selectivity over JAK3 and TYK2.

After all, two thienopyridine derivatives **19** and **22** shared the similarity of the JAK2 selective characteristics. In contrast, it was worth mentioning that the slightly JAK2 selective differences between **19**-JAK and **22**-JAK were mainly ascribed to the interactions in hinge region. The reason may be that the propoxy of **22** can have a greater effect on the hinge region relative to the methyl of **19**. The slight difference also proved the conclusion that the key hinge region served as an important JAK2 selectivity factor.

Table S1. The structure, IC_{50} values and the corresponding scores of RRD docking method for the inhibitor **22**. The italics in the brace mean the fold selectivity *vs.* JAK2.

Compound **22**	Complex	**22**-JAK2	**22**-JAK1	**22**-JAK3	**22**-TYK2
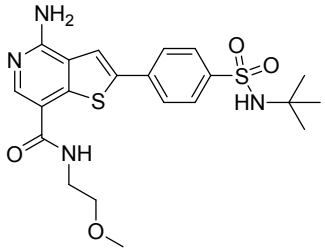	RRD score	-10.943	-5.206	-4.205	-4.073
	pIC_{50} (exp.)	8.52	6.89	5.89	5.83
	IC_{50}(μm)	0.003	0.129(*43*)	1.28(*427*)	1.48(*493*)

Table S2 The predicted binding free energies and the individual energy terms for the complexes **22-**JAK based on MM/GBSA method (kcal mol^{-1}).

Contribution	**22**-JAK2	**22**-JAK1	**22**-JAK3	**22**-TYK2
ΔE_{vdw}	-57.85±2.89	-48.38±2.79	-49.32±2.40	-48.29±3.75
ΔE_{ele}	-32.12±4.84	-47.35±7.14	-12.76±3.12	-22.78±5.25
ΔG_{GB}	40.38±3.93	59.17±4.61	29.20±3.08	37.30±3.83
ΔG_{SA}	-7.33±0.13	-7.07±0.21	-6.35±0.16	-7.04±0.20
ΔG_{MM}	-89.98±5.48	-95.73±7.27	-62.08±3.42	-71.07±5.56
ΔG_{sol}	33.05±3.92	52.10±4.60	22.84±3.07	30.26±3.81
ΔE_{polar}	8.26	11.83	16.44	14.52
$\Delta E_{nonpolar}$	-65.18	-55.46	-55.67	-55.33
ΔG_{pred}	-56.93±3.73	-43.63±4.54	-39.23±3.49	-40.81±4.90
pIC50	8.52	6.89(*43*)	5.89(*427*)	5.83(*493*)

Table S3 Hydrogen bonds analysis for the complexes **22**-JAK from MD simulation.

Complex	Donor	Acceptor	Distance (Å)	Angle (°)	Occupancy (%)
22-JAK2	**22**(N16-H38)	Glu930(O)	2.866	18.31	76.80
	Leu932(N-H)	**22**(N1)	2.915	15.58	54.93
	22(N18-H40)	Leu932(O)	2.895	39.91	27.80
	22(N24-H43)	Asp994(OD1)	2.896	22.31	24.07
22-JAK1	**22**(N24-H43)	Glu883(O)	2.834	16.67	84.33
	22(N16-H38)	Asp1021(OD1)	2.836	24.96	77.07
	22(N16-H39)	Gly1020(O)	2.861	35.03	57.13
	Leu959(N-H)	**22**(O30)	2.888	24.88	18.93
22-JAK3	**22**(N16-H38)	Glu903(O)	2.828	28.07	50.67
	Leu905(N-H)	**22**(N16)	2.926	40.75	17.33
22-TYK2	**22**(N16-H38)	Glu979(O)	2.863	27.77	42.07
	22(N24-H43)	Leu983(O)	2.847	16.98	16.07

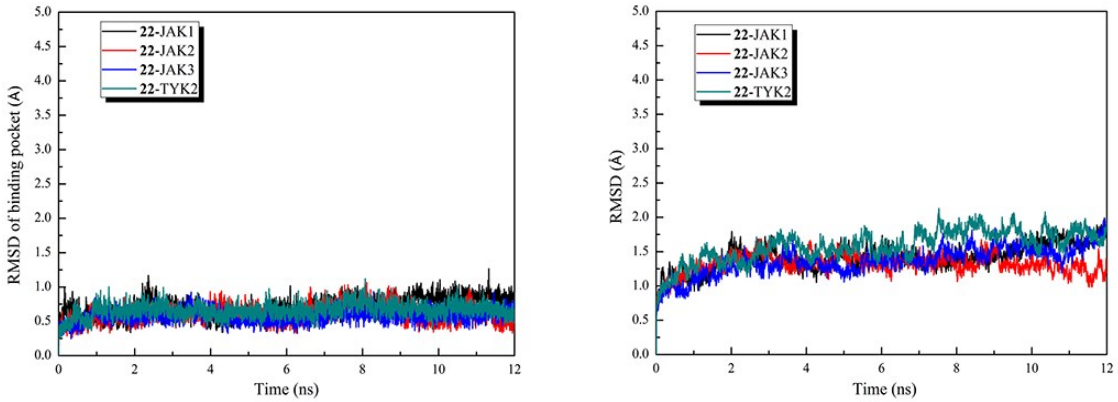

Fig. S2 Time evolution of the RMSD values for four complexes **22**-JAK. (a) C_α atoms for the residues around 5 Å of the ligand; (b) all protein backbone atoms.

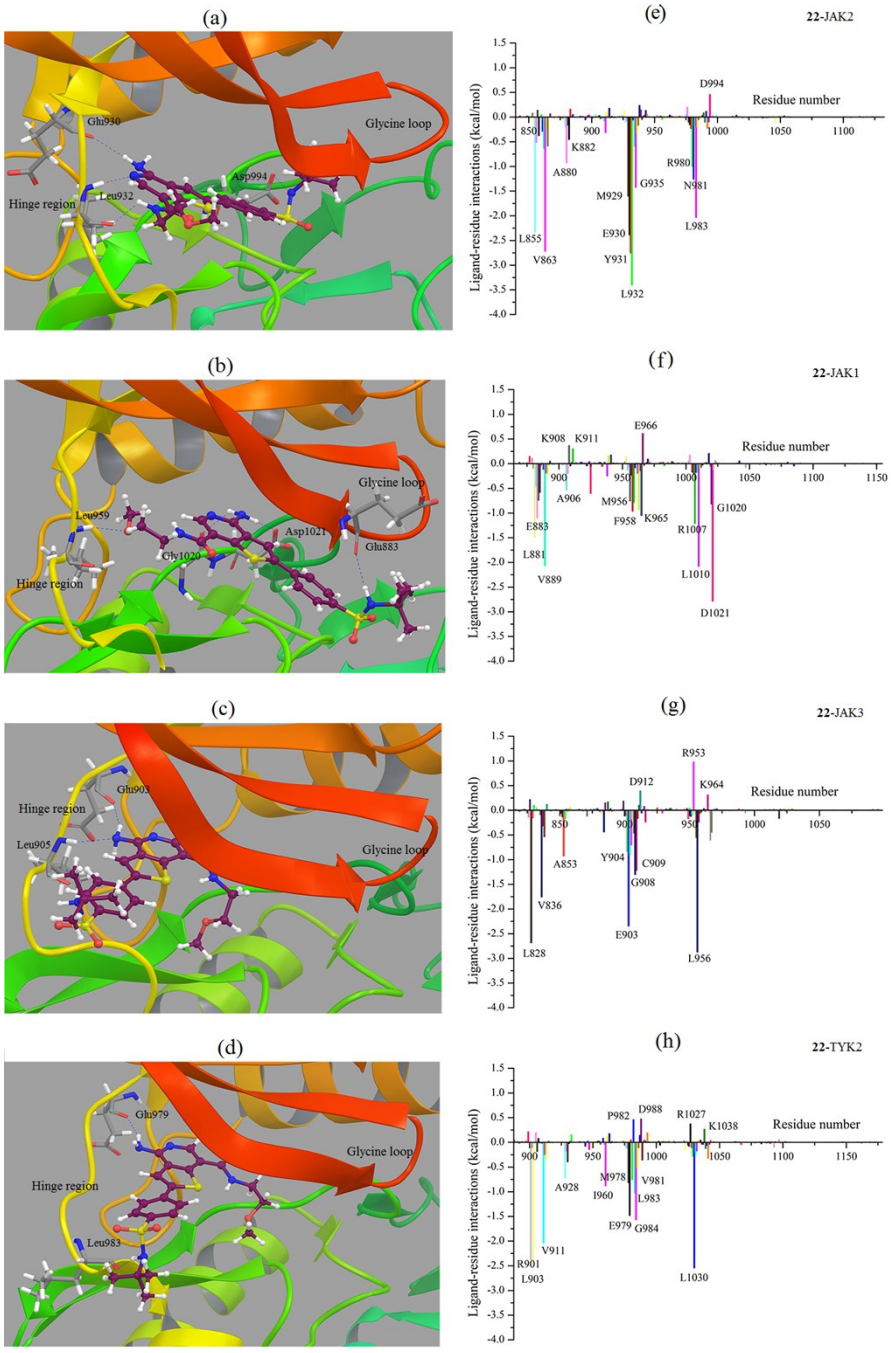

Fig. S3 The predicted modes of the inhibitor **22** binding to the JAK kinases in the active pocket and the corresponding ligand–residue interaction spectra for the complexes **22**-JAK. H-bond interactions were revealed by a blue dotted line. (a) and (e) **22**-JAK2 complex; (b) and (f) **22**-JAK1 complex; (c) and (g) **22**-JAK3 complex; (d) and (h) **22**-TYK2 complex.

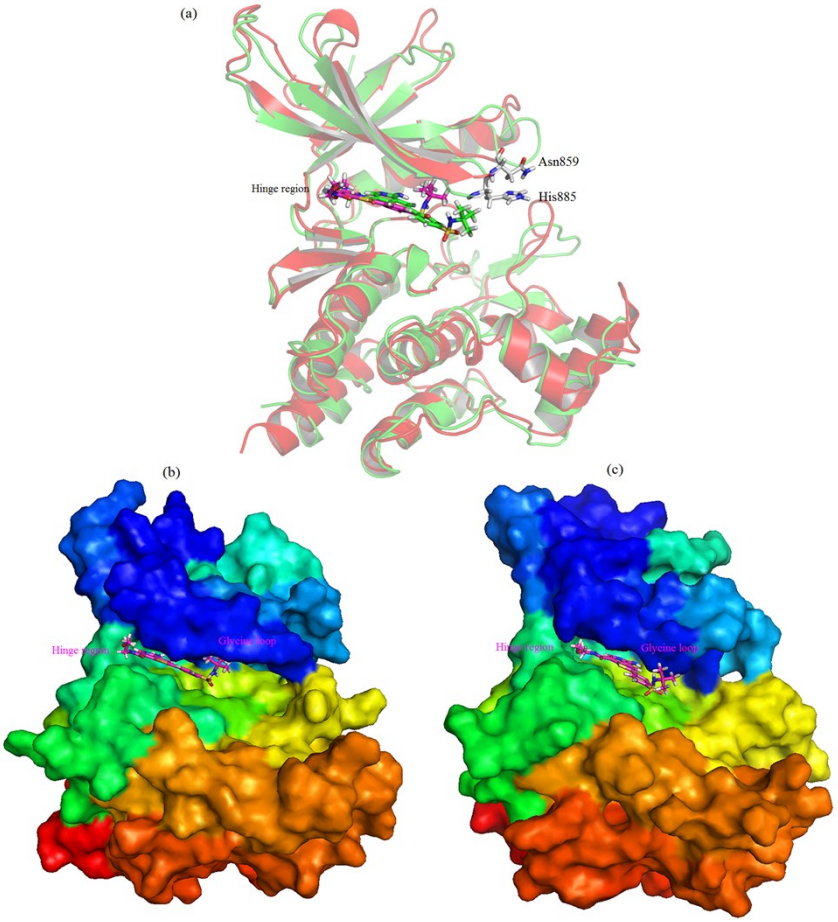

Fig. S4 Comparison of the MD simulation results between complexes **22**-JAK2 (red) and **22**-JAK1 (green) (a). Molecular surface representation of JAK2 PTK (b) and JAK1 PTK (c) in complex with **22**.

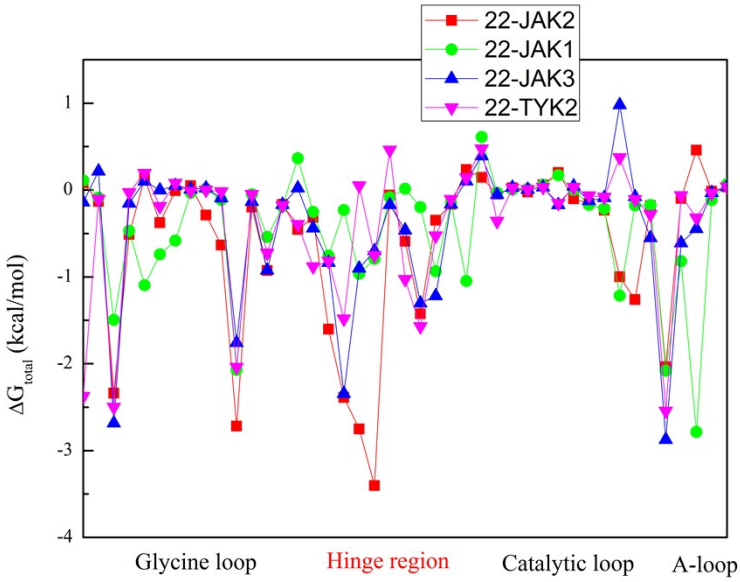

Fig. S5 The per-residue energy contributions of the key domains (the hinge region, glycine-rich loop, catalytic loop and activation loop).

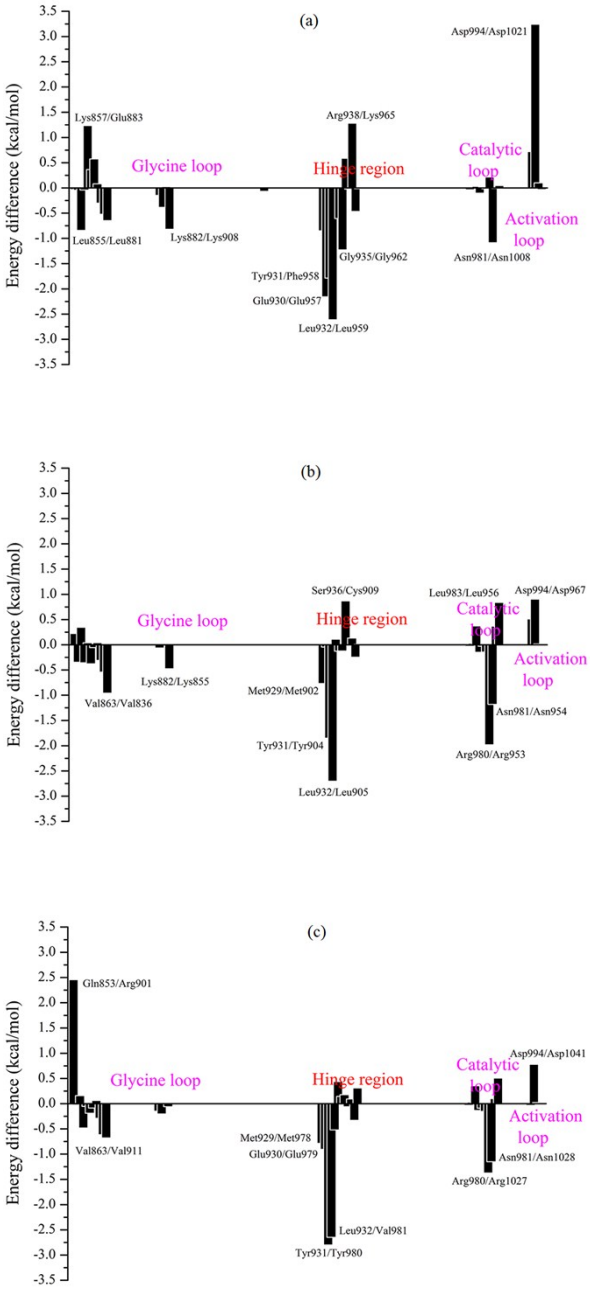

Fig. S6 The energy differences (ΔΔG) of each residue for the complex **22**-JAK2 relative to other complex members **22**-JAK1 (a), **22**-JAK3 (b) and **22**-TYK2 (c).

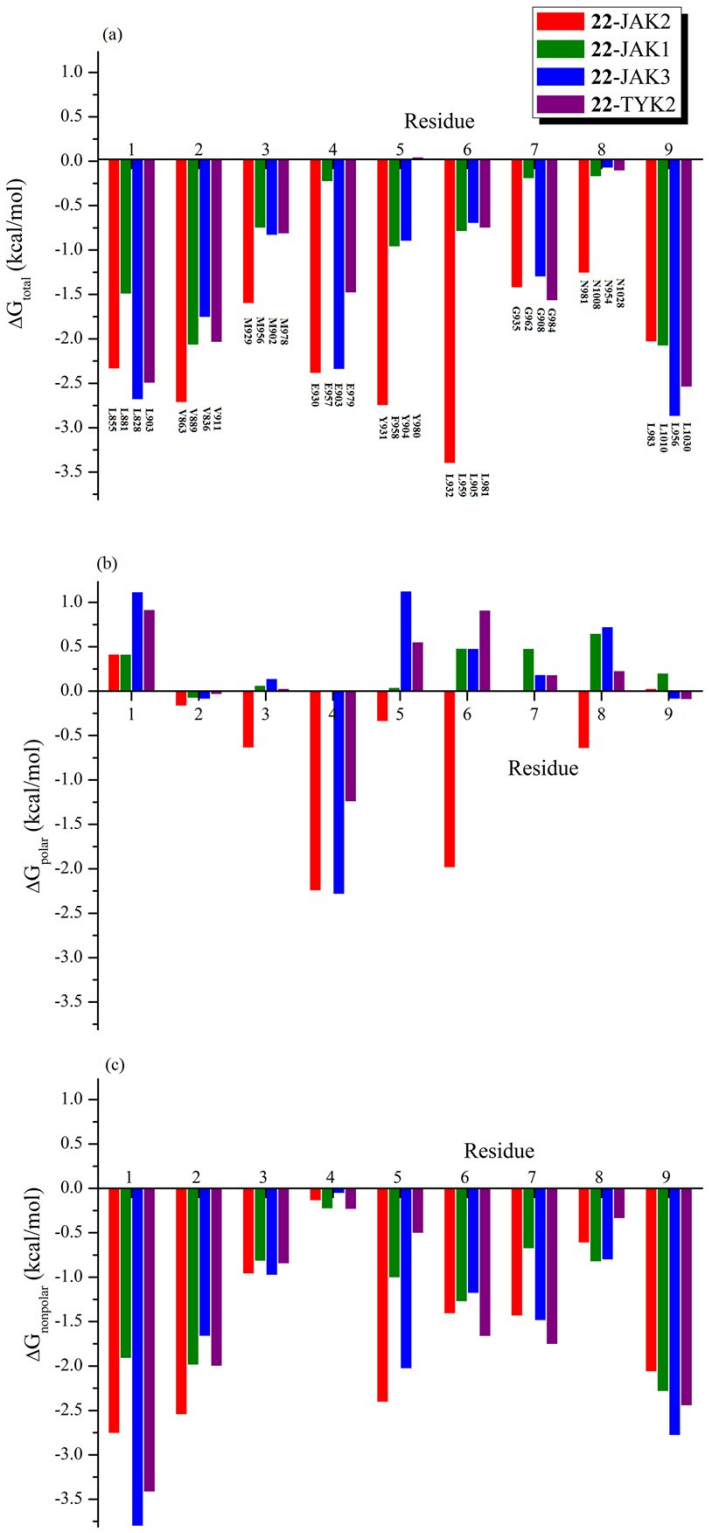

Fig. S7 The key residue interactions for JAK2 kinase and the equivalent residue interactions for JAK1, JAK3 and TYK2. (a) the total binding contributions (ΔG_{total}); (b) the polar contributions (ΔG_{polar}); (c) the nonpolar contributions ($\Delta G_{nonpolar}$).

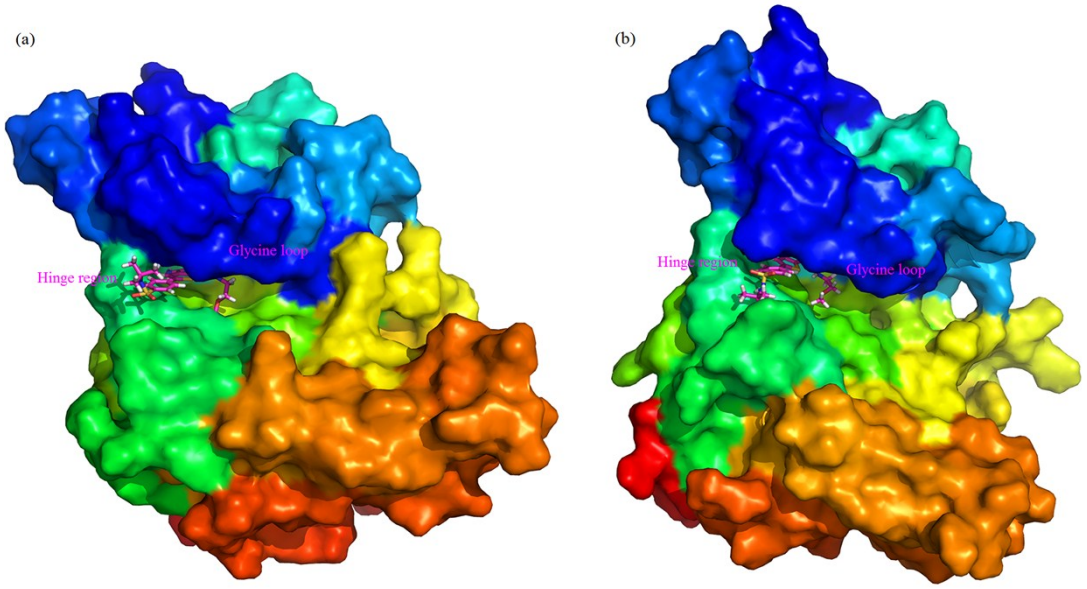

Fig. S8 Molecular surface representation of JAK3 PTK (a) and TYK2 PTK (b) in complex with **22**.

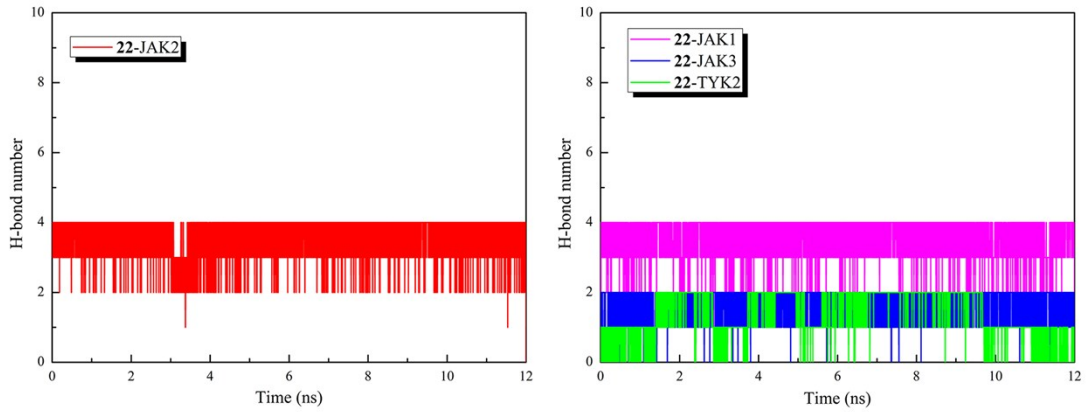

Fig. S9 Numbers of hydrogen bonds *vs.* simulation time for (a) **22**-JAK2 (b) **22**-JAK1, **22**-JAK3 and **22**-TYK2.

3. Supplementary material for the complexes between the new molecules and two kinases JAK2 and JAK1

3.1. Stability of the system simulations

The temporal RMSD values of the C_α atoms of residues within 5 Å around the ligand in the binding pocket and all protein backbone atoms for each system relative to the respective initial structures were convergent, and suggested that all of the systems reached equilibrium after 10 ns

simulation (Fig. S10 and S11). The 300 snapshots were extracted from the last stable 3 ns trajectories to using energy calculations.

3.2. Selectivity analysis for the new molecules

As can be seen in the Table 6, the predicted energy contributions of five ligands-JAK2 systems reached up to -66.69 kcal/mol (-59.37 to -66.69 kcal/mol), and the higher disparities over the corresponding ligands-JAK1 (17.84, 6.02, 16.44, 14.84, 19.12 kcal/mol) indicated that the novel molecules may be the promising activities and high selectivity levels of JAK2 inhibitors (Table S4). The new molecules were stabilized into the active cavity of JAK2 by Van der Wals and electrostatic forces increased markedly. From the surface representation of JAK2 and JAK1 with new molecules (Fig. S12), the compounds in the binding cleft of JAK1 generated certain directed deviations relative to JAK2, which may be the major factor leading to the high JAK2 selectivity. The residues of JAK2 protein in four key domains could be available to act on the new molecules effectively. Owing to the introduction of the R_A and R_B groups, it was not hard to detect the powerful forces in the hinge region at work. The big R_C group was buried suitably in the glycine loop where the residues Lys857 to Gly861 made important contributions to stabilize the complexes. Because of the space structure of the R_A, R_B and R_C groups the scaffold moved down and right slightly and was near to the catalytic loop and activation loop, which formed the favorable interactions between JAK2 and the new molecules (Fig. 10). However, the novel compounds within the complexes ligands-JAK1 could be not fitted into the binding cleft perfectly so that the residue contributions were relatively weak (Fig. S13). The H-bond numbers and interactions of ligands-JAK2 were superior to ligands-JAK1 as well (Table S5 and S6). The MD simulation results provided the valid evidences to verify the reliability and rationality of the new

molecules.

Table S4 The predicted binding free energies and the individual energy terms between the new molecules and JAK1 based on MM/GBSA method (kcal mol^{-1}).

Contribution	**A_1C**-JAK1	**A_3C**-JAK1	**A_3B**-JAK1	**A_3BC**-JAK1	**BC**-JAK1
ΔE_{vdw}	-56.29±4.00	-62.49±2.98	-53.06±2.98	-62.06±3.38	-53.96±3.13
ΔE_{ele}	-52.37±8.16	-56.97±7.21	-21.97±5.98	-45.77±7.05	-14.42±7.66
ΔG_{GB}	74.98±6.07	71.84±5.79	38.87±5.07	64.27±5.61	30.54±6.33
ΔG_{SA}	-7.84±0.25	-7.84±0.19	-6.96±0.24	-8.28±0.36	-7.17±0.22
ΔG_{MM}	-108.67±8.10	-119.46±7.23	-75.03±6.85	-107.83±7.56	-68.39±7.20
ΔG_{sol}	67.14±6.04	64.00±5.73	31.91±4.97	55.98±5.51	23.37±6.36
ΔE_{polar}	22.61	14.87	16.90	18.50	16.12
$\Delta E_{nonpolar}$	-64.13	-70.33	-60.02	-70.34	-61.13
ΔG_{pred}	-41.53±4.20	-55.47±3.77	-43.13±3.75	-51.85±4.45	-45.02±3.87

Table S5 Hydrogen bonds analysis from MD simulation between the new molecules and JAK2.

Complex	Donor	Acceptor	Distance (Å)	Angle (°)	Occupancy (%)
A_1C-JAK2	**A_1C**(N19-H50)	Asp994(OD2)	2.821	19.51	66.60
	Leu932(N-H)	**A_1C**(N1)	2.918	15.07	49.93
	A_1C(N21-H51)	Glu930(O)	2.894	21.88	42.47
	A_1C(N11-H45)	Leu932(O)	2.908	29.82	22.87
A_3C-JAK2	**A_3C**(N21-H52)	Glu930(O)	2.870	23.25	67.93
	A_3C(N19-H51)	Asp994(OD2)	2.823	20.31	58.60
	Leu932(N-H)	**A_3C**(N1)	2.915	16.78	55.73
	A_3C(N11-H46)	Leu932(O)	2.922	25.30	6.13
A_3B-JAK2	**A_3B**(N21-H56)	Glu930(O)	2.877	33.09	66.47
	Leu932(N-H)	**A_3B**(N1)	2.929	15.86	42.87
	A_3B(N11-H41)	Leu932(O)	2.890	40.38	35.27
A_3BC-JAK2	**A_3BC**(N19-H52)	Asp994(OD2)	2.816	33.99	75.73
	A_3BC(N21-H53)	Glu930(O)	2.860	32.50	74.80
	A_3BC(N11-H47)	Leu932(O)	2.881	39.26	44.20
	Leu932(N-H)	**A_3BC**(N1)	2.931	17.70	33.73
	Gln853(NE2-HE21)	**A_3BC**(N29)	2.916	28.31	16.07
BC-JAK2	**BC**(N21-H44)	Glu930(O)	2.885	29.40	56.67
	BC(N19-H43)	Asp994(OD2)	2.835	33.24	50.07
	BC(N11-H38)	Leu932(O)	2.889	35.97	46.87
	Leu932(N-H)	**BC**(N1)	2.929	15.56	42.87

Table S6 Hydrogen bonds analysis from MD simulation between the new molecules and JAK1.

Complex	Donor	Acceptor	Distance (Å)	Angle (°)	Occupancy (%)
A_1C-JAK1	Leu959(N-H)	**A_1C**(O23)	2.843	25.13	67.13
	Glu883(N-H)	**A_1C**(O25)	2.870	17.12	66.33
	A_1C(N21-H52)	Asp1021(OD1)	2.833	23.97	64.47
	A_1C(N19-H50)	Glu883(O)	2.862	28.05	44.73
	A_1C(N21-H51)	Gly1020(O)	2.850	28.48	18.80
A_3C-JAK1	**A_3C**(N40-H64)	Leu959(O)	2.840	28.51	79.47
	A_3C(N21-H51)	Asp1021(OD2)	2.833	30.37	50.00
	Leu959(N-H)	**A_3C**(O23)	2.879	19.62	44.80
	A_3C(N21-H53)	Gly1020(O)	2.866	45.60	44.33
A_3B-JAK1	**A_3B**(N19-H46)	Pro960(O)	2.844	16.49	82.87
	Leu959(N-H)	**A_3B**(N32)	2.937	18.11	11.73
A_3BC-JAK1	Lys909(NZ-HZ1)	**A_3BC**(O22)	2.771	27.27	37.82
	Arg879(NH2-HH21)	**A_3BC**(O32)	2.857	37.78	4.71
BC-JAK1	**BC**(N21-H44)	Leu959(O)	2.828	26.10	84.13
	Leu959 (N-H)	**BC**(N1)	2.939	18.87	19.60

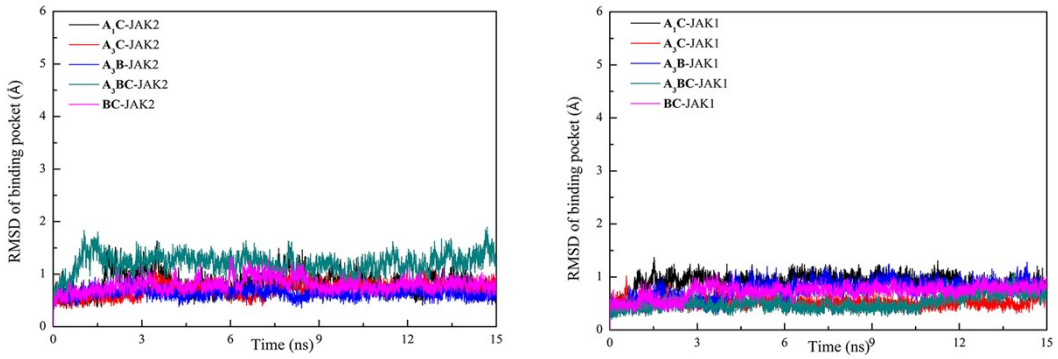

Fig. S10 Time evolution of the RMSD values of C_α atoms for the residues around 5 Å of the ligand.

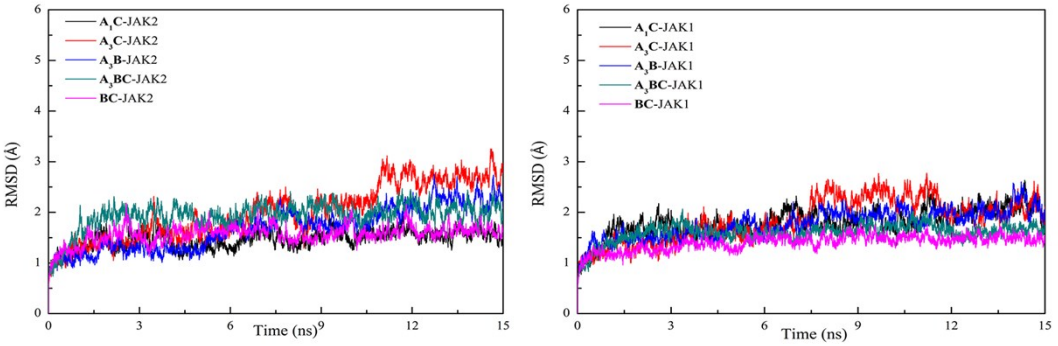

Fig. S11 Time evolution of the RMSD values of all protein backbone atoms

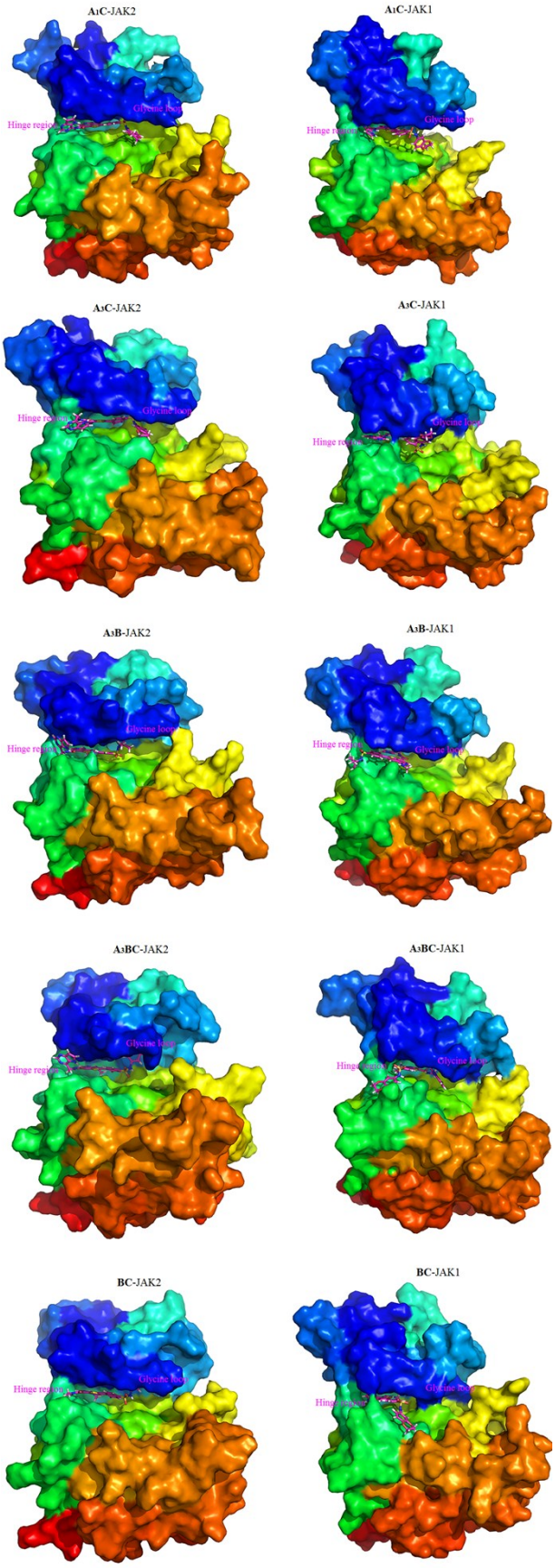

Fig. S12 Molecular surface representation between the new molecules and the kinases JAK2 and JAK1.

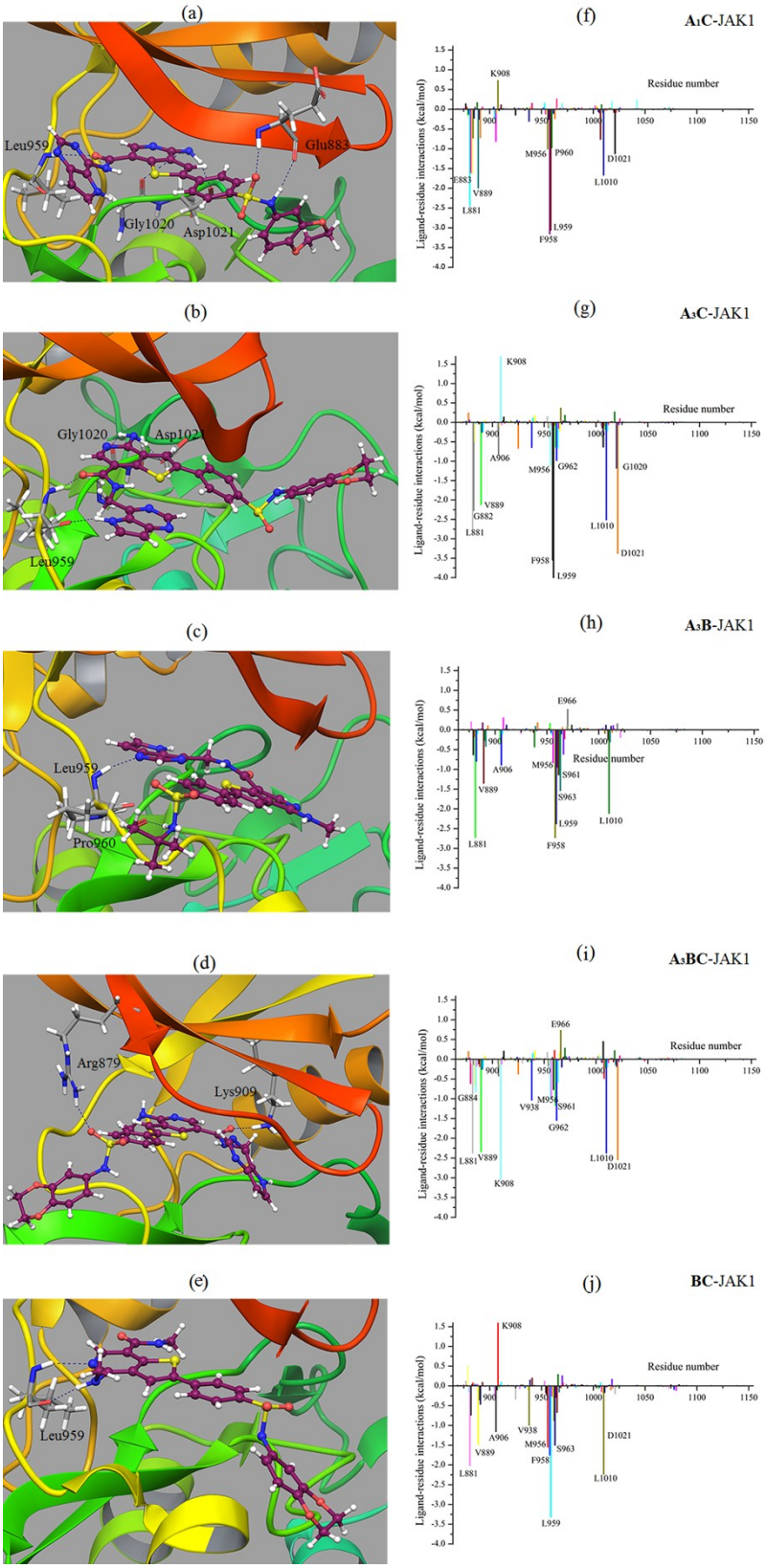

Fig. S13 The predicted modes of the new molecules binding to JAK1 in the active pocket and the corresponding ligand–residue interaction spectra for the complexes**.** H-bond interactions were revealed by a blue dotted line.